PHYSICAL REVIEW D **94,** 103518 (2016)

Dynamics of neutrino lumps in growing neutrino quintessence

Santiago Casas,[*] Valeria Pettorino,[†] and Christof Wetterich[‡]
Institut für Theoretische Physik, Ruprecht-Karls-Universität Heidelberg, Philosophenweg 16, 69120 Heidelberg, Germany
(Received 15 August 2016; published 18 November 2016)

We investigate the formation and dissipation of large-scale neutrino structures in cosmologies where the time evolution of dynamical dark energy is stopped by a growing neutrino mass. In models where the coupling between neutrinos and dark energy grows with the value of the scalar cosmon field, the evolution of neutrino lumps depends on the neutrino mass. For small masses the lumps form and dissolve periodically, leaving only a small backreaction of the neutrino structures on the cosmic evolution. This process heats the neutrinos to temperatures far above the photon temperature, such that neutrinos acquire again an almost relativistic equation of state. The present equation of state of the combined cosmon-neutrino fluid is very close to -1. By contrast, for larger neutrino masses, the lumps become stable. The highly concentrated neutrino structures entail a large backreaction similar to the case of a constant neutrino-cosmon coupling. A present average neutrino mass of around 0.5 eV seems to be compatible with observations so far. For masses lower than this value, neutrino-induced gravitational potentials remain small, making the lumps difficult to detect.

DOI: 10.1103/PhysRevD.94.103518

I. INTRODUCTION

The observed accelerated expansion of the Universe is currently well described by the standard lambda cold dark matter (ΛCDM) scenario, where a cosmological constant leads the background of the Universe to a final de Sitter state. Such a scenario, however, raises a "coincidence" (or "why-now") problem, as it is not understood why dark energy has become important only recently, marking the present cosmological epoch as a special one within cosmic history. Alternative models of dynamical dark energy or modified gravity should address the why-now problem and the associated fine-tuning of parameters. At the same time, these models need to explain why dark energy is almost static in the present epoch, such that the present dark energy equation of state w is close to the observed range near -1.

Growing neutrino quintessence [1,2] explains the end of a cosmological scaling solution (in which dark energy scales as the dominant background) and the subsequent transition to a dark energy dominated era by the growing mass of neutrinos, induced by the change of the value of the cosmon field which is responsible for dynamical dark energy. The dependence of the mass of neutrinos on the cosmon (dark energy) field ϕ,

$$m_\nu = m_\nu(\phi) \propto \hat{m}_\nu e^{-\int \beta(\phi) d\phi}, \qquad \beta(\phi) = -\frac{\partial \ln m_\nu(\phi)}{\partial \phi}, \tag{1}$$

involves the cosmon-neutrino coupling $\beta(\phi)$, which measures the strength of the fifth force (additional to gravity). The constant $\hat{m}_\nu$ is a free parameter of the model which determines the size of the neutrino mass. (We take, for simplicity, all three neutrino masses equal—or, equivalently, m_ν stands qualitatively for the average over the neutrino species.) The special role of the neutrino masses (as compared to quark and charged lepton masses) is motivated at the particle physics level by the way in which neutrinos get masses [2]. Growing neutrino quintessence with a sufficiently large negative value of β successfully relates the present dark energy density and the mass of the neutrinos. The evolution of the cosmon is effectively stopped once neutrinos become nonrelativistic. Dark energy becomes important now because neutrinos become nonrelativistic in a rather recent past, at typical redshifts of about $z = 5$ [3]. In this way, the why-now problem is resolved in terms of a "cosmic trigger event" induced by the change in the effective neutrino equation of state, rather than by relying on the fine-tuning of the scalar potential. This differs from other mass-varying neutrino cosmologies [4–10]. Some of the observational consequences of those models were studied in [5,8] and, more recently, a new scalar field–neutrino coupling that produces viable cosmologies was proposed in [11]. A viable cosmic background evolution of growing neutrino quintessence offers interesting prospects for the possible observation of the neutrino background.

The case in which the coupling β is constant has been largely investigated in the literature at the linear level [3], in semianalytical nonlinear methods [12–14], joining linear and nonlinear information to test the effect of the neutrino lumps on the cosmic microwave background [15] and

[*]casas@thphys.uni-heidelberg.de
[†]v.pettorino@thphys.uni-heidelberg.de
[‡]c.wetterich@thphys.uni-heidelberg.de

within N-body simulations [16–19]. For the values of β ($\beta \gtrsim 10^3$) needed for dark energy to dominate today, the cosmic neutrino background is clumping very fast. Large and concentrated neutrino lumps form and induce very substantial backreaction effects. These effects are so strong that the deceleration of the evolution of the cosmon gets weak, making it difficult to obtain a realistic cosmology [20].

In this paper, we instead consider the case in which the neutrino-cosmon coupling $\beta(\phi)$ depends on the value of the cosmon field and increases with time. In a particle physics context, this has been motivated [2] by a decrease with ϕ of the heavy mass scale (the baryon-lepton-violating scale) entering inversely the light neutrino masses. In this scenario, $\beta(\phi)$ has not been large in all cosmological epochs—the present epoch corresponds to a crossover where β gets large. A numerical investigation [18] of this type of model has revealed compatibility with observations for the case of a neutrino mass $m_{\nu,0} = 0.07$ eV. In this paper we investigate the dependence of cosmology on the value of the neutrino mass by varying the parameter $\hat{m}_\nu$ in Eq. (1). For large neutrino masses, we find a qualitative behavior similar to the case of a constant neutrino-cosmon coupling β, with difficulties in obtaining a realistic cosmology. In contrast, for a small neutrino mass, the neutrino lumps form and dissolve, with little influence on the overall cosmological evolution. In this case, the neutrino-induced gravitational potentials are found to be much smaller than the ones induced by dark matter. As we will discuss in this paper, it will not be easy to find observational signals for the neutrino lumps. Between the regions of small and large neutrino masses, we expect a transition region for intermediate neutrino masses where, by continuity, observable effects of the neutrino lumps should show up.

II. GROWING NEUTRINOS WITH VARYING COUPLING

We consider here cosmologies in which neutrinos have a mass that varies in time, along the framework of "varying growing neutrino models" [2]. As long as neutrinos are relativistic, the coupling is inefficient and the dark energy scalar field ϕ rolls down a potential, as in an early dark energy scenario. As the neutrino mass increases with time, neutrinos become nonrelativistic, typically at a relatively late redshift $z \approx 4$–6 [15]. This influences the evolution of ϕ, which feels the effect of neutrinos via a coupling to the neutrino mass $m_\nu(\phi)$. The evolution of the scalar field slows down and practically stops, such that the potential energy of the cosmon behaves almost as a cosmological constant at recent times. In other words, in these models the cosmological constant behavior observed today is related to a cosmological trigger event (i.e., neutrinos becoming nonrelativistic), and the present dark energy density is directly connected to the value of the neutrino mass. In the following we will detail the formalism and the equations used to describe the cosmological evolution of the model.

We start with the linearized Friedman-Lemaître-Robertson-Walker metric in the Newtonian gauge:

$$ds^2 = -(1+2\Psi)dt^2 + a^2(1-2\Phi)d\mathbf{x}^2. \tag{2}$$

Moreover, we use a quasistatic approximation for subhorizon scales ($H/k \ll 1$), which allows us to neglect time derivatives with respect to spatial ones. Then the quasistatic, first-order perturbed Einstein equations are the Poisson equation [21]

$$k^2\Phi = 4\pi G a^2 \delta T^0_0, \tag{3}$$

and the "stress" equation

$$k^2(\Phi - \Psi) = 12 G a^2(\bar{\rho} + \bar{P})\sigma, \tag{4}$$

where δT^0_0 is the perturbation of the 0–0 component of the energy-momentum tensor $T_{\mu\nu}$ and σ is the anisotropic stress of the fluid which depends on the traceless component of the spatial part of the energy-momentum tensor, $T^i_j - \delta^i_j T^k_k/3$. This stress tensor is, in our case, only important for relativistic particles (i.e., the neutrinos). The source term of the Poisson equation (3) will contain contributions from all matter species (dark matter and neutrinos) and from the cosmon field. It is proportional to the total density contrast $\delta\rho_t = \delta\rho_\nu + \delta\rho_m + \delta\rho_\phi$.

The cosmon field can be described through a Lagrangian in the standard way,

$$-\mathcal{L}_\phi = \frac{1}{2}\partial^\nu\phi\partial_\nu\phi + V(\phi), \tag{5}$$

where, for this work, we choose an exponential potential $V(\phi) \propto e^{-\alpha\phi}$. The field-dependent mass [Eq. (1)] allows for an energy-momentum transfer between neutrinos and the cosmon, which is proportional to the trace of the energy-momentum tensor of neutrinos $T_{(\nu)}$ and to a coupling parameter $\beta(\phi)$:

$$\nabla_\eta T^{\mu\eta}_{(\phi)} = +\beta(\phi)T_{(\nu)}\partial^\mu\phi, \tag{6}$$

$$\nabla_\eta T^{\mu\eta}_{(\nu)} = -\beta(\phi)T_{(\nu)}\partial^\mu\phi. \tag{7}$$

The cosmon is the mediator of a fifth force between neutrinos, acting at cosmological scales. Its evolution is described by the Klein-Gordon equation sourced by the trace of the energy-momentum tensor $T_{(\nu)}$ of the neutrinos,

$$\nabla_\mu\nabla^\mu\phi - V'(\phi) = \beta(\phi)T_{(\nu)}. \tag{8}$$

As long as the neutrinos are relativistic [$T_{(\nu)} = 0$], the source on the right-hand side vanishes. During this time,

the coupling has no effect on the evolution of ϕ. While the potential term $\sim V'$ drives ϕ towards larger values, the term $\sim\beta$ has the opposite sign and stops the evolution effectively once $\beta T_{(\nu)}$ equals V'. The trace of the energy-momentum tensor T_ν, entering Eq. (8), is equal to

$$T_\nu = m_\nu(\phi)\tilde{n}(\phi), \tag{9}$$

where $\tilde{n}_\nu(\phi) = n_\nu(\phi)/\gamma$ is the ratio of the number density of neutrinos n_ν divided by the relativistic γ factor. Equation (9) is valid for both relativistic and nonrelativistic neutrinos. Here, we consider a coupling β between neutrino particles and the quintessence scalar field ϕ as a field-dependent quantity:

$$\beta(\phi) \equiv -\frac{1}{\phi_c - \phi}. \tag{10}$$

From Eq. (1), the neutrino mass is then given by

$$m_\nu(\phi) = \frac{\bar{m}_\nu}{\phi_c - \phi}. \tag{11}$$

Here, ϕ_c denotes the asymptotic value of ϕ for which β and $m_\nu(\phi)$ would formally become infinite. By an additive shift in ϕ, it can be set to an arbitrary value, e.g., $\phi_c = 0$. We consider the range $\phi < \phi_c$. The divergence of β for $\phi \to \phi_c$ in Eq. (10) is not crucial for the results of this paper—β and m_ν never increase to large values, such that the immediate vicinity of ϕ_c plays no role.

The coupling induces a total force acting on neutrinos given by $\nabla(\Phi_\nu + \beta\delta\phi)$ and appearing in the corresponding Euler equation [15], as is typical in coupled cosmologies [22]. For values $2\beta^2 > 1$, the fifth force induced on neutrinos by the cosmon becomes larger than the gravitational attraction. For the large values of $|\beta| \approx 10^2$ reached during the cosmological evolution, the attraction induced by the cosmon gives rise to the formation of neutrino lumps. As shown in [3,15], this represents the major difficulty encountered within growing neutrino models and also, simultaneously, one of its clearest predictions with respect to alternative dark energy models: the presence of neutrino lumps at scales of ≈10 Mpc or even larger, depending on the details of the model [3]. Since the attractive force between neutrinos is 10^4 times bigger than gravity, the dynamical time scale of the clumping of neutrino inhomogeneities is also, therefore, a factor of 10^4 faster than the gravitational time scale. Even the tiny inhomogeneities in the cosmic neutrino background grow very rapidly nonlinear. The impact of such structures has been shown to depend crucially on the strength of backreaction effects [17,19]. For constant coupling, the effect of backreaction is strong and can lead to neutrino lumps with rapidly growing concentration, reaching values of the gravitational potential which exceed the observational constraints. The effect is so strong that it is able to destroy the oscillatory effect first encountered in [22], in which neutrino lumps were forming and then dissipating. No realistic cosmology has been found in this case [20]. With the varying coupling of Eq. (10), a similar behavior will be found for large neutrino masses. For small neutrino masses, the oscillatory effects will be dominant and realistic cosmologies seem possible [19].

III. NUMERICAL TREATMENT OF GROWING NEUTRINO COSMOLOGIES

A. Modified Boltzmann code

For the early stages of the evolution of the growing neutrino quintessence model, neutrinos behave as standard relativistic particles and the coupling to the cosmon field is suppressed. Therefore, the Klein-Gordon equation can be linearized and no important backreaction effects are present. The Einstein-Boltzmann system of equations for the relativistic neutrinos and all other species has been solved using a modified version of the code CAMB [23] (hereafter referred to as nuCAMB), used and developed already in previous papers on mass-varying and growing neutrino cosmologies. We refer the reader to previous publications [3,4,13,15] for details about the implementation of nuCAMB. These equations are valid until neutrinos become nonrelativistic and as long as perturbations are still linear. The neutrinos can be seen as a weakly interacting gas of particles in thermal equilibrium with a phase-space distribution $f(p)$, with p denoting the momentum. The statistical description is, in the case of neutrinos, a Fermi-Dirac distribution, given by

$$f_{\rm FD}(p) = \frac{1}{e^{(E(p)-\mu)/T} + 1}, \tag{12}$$

where μ is the chemical potential and $E(p) = \sqrt{m^2 + p^2}$ the particle energy. Then the number density of neutrinos, the energy density, and the pressure are given, respectively, by

$$n_\nu = \frac{2}{(2\pi)^3}\int \mathrm{d}^3 p f_{\rm FD}(p), \tag{13}$$

$$\rho_\nu = \frac{2}{(2\pi)^3}\int \mathrm{d}^3 p E(p) f_{\rm FD}(p), \tag{14}$$

$$P_\nu = \frac{2}{(2\pi)^3}\int \mathrm{d}^3 p \frac{p^2}{E(p)} f_{\rm FD}(p). \tag{15}$$

The solution of the Boltzmann hierarchy of neutrinos coupled to the perturbed Einstein equations (3) and (4), together with the solution of the background Klein-Gordon equation (8), form the basis of the modification of nuCAMB with respect to the standard code CAMB, which

TABLE I. Table of parameters for the six models considered in this work. The top part refers to the output values computed with the linear nuCAMB code. The bottom part refers to values computed within the N-body simulation. Quantities denoted with a subscript 0 are values at the present time, $a = 1.0$. The $\langle m_\nu\rangle[a_1 : a_2]$ is the root mean squared (rms) value of the neutrino mass in units of eV computed between $a = a_1$ and $a = a_2$. The same notation is also valid for $\langle w_{\nu\phi}\rangle[a_1, : a_2]$ corresponding to the equation of state of the combined cosmon and neutrino fluid which represents dynamical dark energy. $a_{\rm final}$ is the final time at which simulations were computed accurately. Therefore, for the models M3–M6 we cannot cite values of present time quantities or averages at times beyond $a_{\rm final}$. The input values for nuCAMB corresponding to all of the models can be found in Table II of Appendix A.

Cosmological parameters	Growing neutrino models					
Linear values	M1	M2	M3	M4	M5	M6
$\Omega_{\nu 0} + \Omega_{\phi 0}$	0.686	0.688	0.692	0.701	0.693	0.697
$\Omega_{\nu 0}$	3.8×10^{-3}	2.6×10^{-2}	1.64×10^{-2}	4.7×10^{-2}	6.1×10^{-2}	9.4×10^{-2}
h	0.671	0.673	0.6818	0.701	0.722	0.740
$m_{\nu 0}$ (eV)	0.060	0.407	0.239	0.730	1.000	1.712
$\langle m_\nu\rangle[0.4:0.6]$ (eV)	0.040	0.067	0.134	0.277	0.399	0.701
$\langle m_\nu\rangle[0.8:1.0]$ (eV)	0.099	0.152	0.318	0.661	0.907	1.51
$\langle w_{\nu\phi}\rangle[0.9:1.0]$	−0.97	−0.97	−0.95	−0.92	−0.90	−0.85
N-body values						
$\Omega_{\nu 0} + \Omega_{\phi 0}$	0.688	0.690	...	...	...	...
$\Omega_{\nu 0}$	2.5×10^{-2}	1.9×10^{-2}	...	...	...	...
$m_{\nu 0}$ (eV)	0.038	0.078	...	...	...	...
$\langle m_\nu\rangle[0.4:0.6]$ (eV)	0.048	0.069	0.1436	0.280	0.401	0.676
$\langle m_\nu\rangle[0.8:1.0]$ (eV)	0.120	0.164	...	...	...	...
$\langle w_{\nu\phi}\rangle[0.9:1.0]$	−0.95	−0.96	...	...	...	...
$a_{\rm final}$	1.0	1.0	0.84	0.70	0.65	0.67

handles dark matter, photons, and baryons altogether. We recall that, for growing neutrino quintessence, the neutrino mass depends on the cosmon field ϕ and, therefore, on the scale factor a.

The ratio of the initial mass of the neutrinos to their temperature (given in eV) is calculated in nuCAMB as follows:

$$\hat{r}_{\nu\mathrm{eV}} \equiv \left(\frac{m}{T}\right)_{\nu,\mathrm{camb}} = \frac{(7/8)(\pi^4/15)}{(3/2)\zeta(3)} \times \frac{\rho_{\rm cr}\Omega_{\nu,\mathrm{input}}}{\rho_\nu}. \tag{16}$$

The first fraction comes from the relation $m_\nu \approx \rho_\nu/n_\nu = ((\frac{7}{8}\frac{\pi^4}{15})/\frac{3}{2}\zeta(3))T_\nu$, which is valid in the nonrelativistic limit of Eqs. (12)–(15); the critical density is defined as usual: $\rho_{\rm cr} = \frac{3H^2_{0,\mathrm{input}}}{8\pi G}$. The second fraction is a rescaling that corrects the neutrino density in order to match the wanted $\Omega_{\nu,\mathrm{input}}$ given as an input value. The code performs an iterative routine that varies the initial conditions in such a way that the input parameters are obtained at the present time. Since this is not exact, the final values of H_0 and Ω_ν might vary slightly with respect to the given input values. The ratio $\hat{r}_{\nu\mathrm{eV}}$ depends on the input parameters $H_{0,\mathrm{input}}$ (via the critical density) and on $\Omega_{\nu,\mathrm{input}}$.[1] Furthermore, the neutrino energy density ρ_ν and the photon energy density ρ_γ at relativistic times are related as

$$\rho_\nu = N_\nu \times \frac{7}{8} \times \left(\frac{4}{11}\right)^{4/3} \rho_\gamma, \tag{17}$$

where $N_\nu = 3$ is the number of neutrino species. The use of these formulas is valid if initial conditions are set when neutrinos are nonrelativistic, where the linear regime still applies. For initial conditions set at an earlier time, relativistic corrections have to be taken into account. After solving the Einstein-Boltzmann system, realizations of the fields $\delta_\nu(\mathbf{k})$ and $v_{\mathrm{pec},\nu}(\mathbf{k})$ at an early time are obtained from nuCAMB and are then used as the initial conditions for the neutrino distribution in the growing neutrino quintessence N-body simulation. This will be explained in more detail at the end of the following section.

B. N-body simulation

For N-body simulations, we use here the code developed in [16,17,19] and then refined in [20] and in the present work, which uses a particle-mesh approach for the neutrino and dark matter particle evolution and a multigrid approach for solving the nonlinear scalar field equations. In Table I we describe the parameters of the models discussed in this paper. We consider five models with different neutrino masses.

Our N-body simulation differs from standard Newtonian N-body codes in many ways, the most important one being that we evolve the cosmon ϕ and the gravitational potentials Φ and Ψ separately. While neutrinos, dark matter, and the cosmon are nonlinear in the N-body simulations, we

[1] $\hat{r}_{\nu\mathrm{eV}}$ is also the conversion factor between the mass units in the N-body code and units in eV.

assume that the gravitational potentials Φ and Ψ are small, which is valid in cosmological applications, even for large deviations of standard ΛCDM and at small scales. The perturbation in the dark energy scalar field $\delta\rho_\phi$ can be calculated from the perturbation of the energy density of the cosmon field

$$\delta\rho_\phi = \frac{\bar{\phi}'\delta\phi}{a^2} + V(\bar{\phi})\delta\phi. \tag{18}$$

The evolution of the homogeneous potential of the cosmon field can be obtained through its energy density and pressure in the following way:

$$V_\phi(a) = \frac{1}{2}(\rho_\phi(a) - p_\phi(a)), \tag{19}$$

while the perturbations in the potential can be approximated by

$$\delta V_\phi(a) = -\frac{1}{2}(\delta\rho_\phi(a) + 3\delta p_\phi(a)). \tag{20}$$

The cosmon field can cluster and, therefore, its spatial gradients are nonvanishing, so that, after averaging over the volume of the box, the energy density of the cosmon field is

$$\bar{\rho}_\phi = \frac{1}{2}\overline{\dot{\phi}^2} + \frac{1}{2a^2}\overline{(1+2\Phi)\partial_i\phi\partial_j\phi\delta^{ij}} + \overline{V(\phi)}, \tag{21}$$

while its pressure reads

$$\bar{P}_\phi = \frac{1}{2}\overline{\dot{\phi}^2} - \frac{1}{6a^2}\overline{(1+2\Phi)\partial_i\phi\partial_j\phi\delta^{ij}} + \overline{V(\phi)}. \tag{22}$$

We will use for the following a convention in which bars denote spatial averages, while angular brackets denote time averaged quantities. The evolution of the cosmon field is solved using a multigrid relaxation algorithm, known as the Newton-Gauß-Seidel (NGS) solver, which was originally developed for $f(R)$ modified gravity simulations [24] and has also been implemented into the growing neutrino N-body simulations in [19]. The bottom part of Table I lists the results of the six models computed using the N-body simulations.

In the case of neutrinos, the mass is a time-varying quantity following Eq. (11). Neutrinos obey a modified geodesic equation,

$$\frac{du^\mu}{d\tau} + \Gamma^\mu_{\nu\lambda}u^\nu u^\lambda = \beta(\phi)\partial^\mu\phi + \beta(\phi)u^\nu u^\mu\partial_\nu\phi, \tag{23}$$

in which the right-hand side gets a contribution from the coupling.

Simulations start at an initial value of $a_{\rm in} = 0.02$. Up until $a \approx 0.30$, the dark matter particles, the cosmon field, and the gravitational potentials are evolved on the grid. For dark matter particles, we take the standard initial conditions from nuCAMB and start the particle-mesh algorithm that solves the Poisson equation (3) at an initial redshift of $z = 49$. This is not the most accurate way of setting initial conditions for cosmological dark matter simulations (see, for example, the recent N-body comparisons in [25]), but since in this work we are not interested in detailed substructures of dark matter halos or a percent-accurate power spectrum, we find that our approach gives a correct description at the scales of interest. Neutrinos are first treated differently from other particles, as a distribution of relativistic particles in thermal equilibrium and no backreaction effects from neutrino structures are taken into account. Starting from a scale factor of approximately $a_{\rm ini} \approx 0.30$ (depending on the exact parameters of each model), which is when neutrinos become nonrelativistic, neutrinos are also projected on the grid: their phase-space distribution is sampled using effective particles. Since their equation of state is nonrelativistic, we can approximate the phase-space distribution by

$$f_\nu(\mathbf{x},\mathbf{v}) = \bar{n}_\nu f_{\rm FD}(|\mathbf{v}_\nu - \mathbf{v}_{\mathbf{pec},\nu}(\mathbf{x})|)(1+\delta_v(\mathbf{x})), \tag{24}$$

where $f_{\rm FD}$ is the Fermi-Dirac distribution (12). The thermal velocities of the neutrinos are the difference between their total velocities and their peculiar velocities $\mathbf{v}_{{\rm th},\nu} = \mathbf{v}_\nu - \mathbf{v}_{{\rm pec},\nu}$. We obtain $\delta_v(\mathbf{x})$ and $\mathbf{v}_{\mathbf{pec},\nu}(\mathbf{x})$ by Fourier transforming the momentum-space realization of those fields obtained at the time $a_{\rm ini}$ from nuCAMB. Equation (24) is solved for $\mathbf{v}_{{\rm th},\nu}$ in order to obtain the correct thermal distribution of particles and we duplicate the number of neutrino particles in each grid, assigning to each of them a thermal velocity which is equal in magnitude but opposite in direction, to avoid a distortion of the distribution of peculiar velocities at larger scales than a single grid cell size. For a large enough number of effective neutrino particles (i.e., when there is much more than one particle per cell), the distortion of the peculiar velocities by thermal velocities should be negligible. The correct neutrino density one would obtain from the Fermi-Dirac distribution for a nonrelativistic particle reads

$$\langle\rho_\nu(\mathbf{x})\rangle_{f_\nu} = \int {\rm d}^3v m_\nu f_\nu(\mathbf{x},\mathbf{v}) = m_\nu\bar{n}_\nu(1+\delta_v(\mathbf{x})). \tag{25}$$

Since we need to enforce the right-hand side of (25) at each grid cell of comoving volume $a^3\Delta V$, where the mass of the neutrinos is given by the scalar field, we have a condition on the number of particles $N_{\rm part}$, such that

$$\frac{M_\nu\langle N_{\rm part}\rangle}{a^3\Delta V} = m_\nu\bar{n}_\nu(1+\delta_v(\mathbf{x})), \tag{26}$$

is fulfilled (more details of these methods can be found in [17]). When neutrinos enter as particles into the N-body simulation and, therefore, backreaction effects from neutrino structures start becoming important, the calculation of

the fields and the potentials becomes computationally demanding due to the nonlinearity of the terms sourcing the continuity (7) and Klein-Gordon equations (8). Since these equations cannot be linearized due to the large values of the coupling parameter $\beta(\phi)$, the multigrid Newton-Gauß-Seidel solver is of crucial importance. For the parallelization of the code, we use a simple OpenMP approach, which calculates in parallel, for the available processing cores, the equations of motion of the particles, and the fast Fourier transforms. In Table III we describe all of the parameters related to the N-body simulations, including box and grid size.

IV. LUMP DYNAMICS AND THE LOW MASS–HIGH MASS DIVIDE

We find two different regimes for the nonlinear evolution of neutrino lumps, depending on the average value of the neutrino mass. For light neutrino masses during the lump formation process, the neutrinos are accelerated to

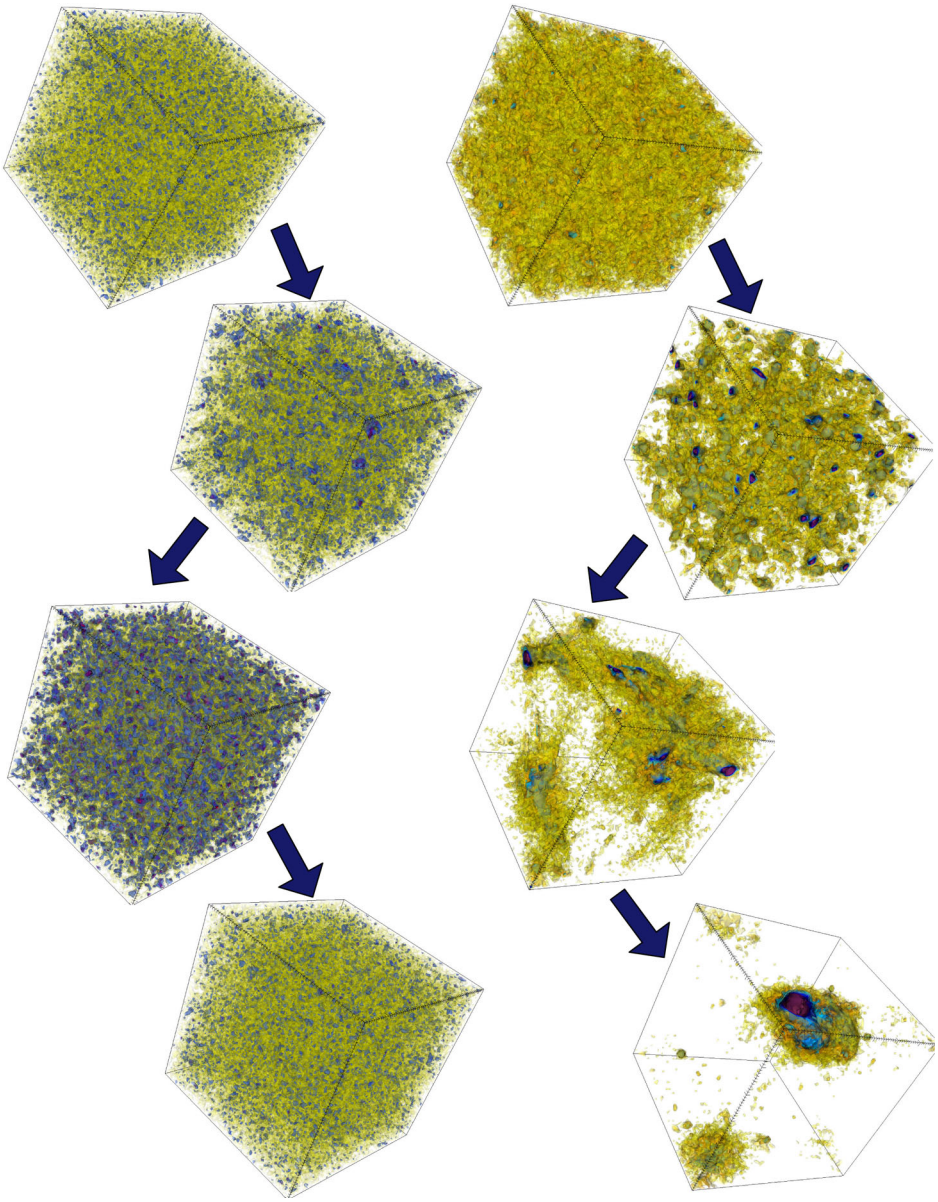

FIG. 1. Snapshots of the number density contrast of neutrinos $\delta n_\nu(\vec{x}) \equiv n_\nu(\vec{x})/\bar{n}_\nu - 1$ at different times. (Left panel) Model M2, at scale factors $a = 0.45, 0.7, 0.75$, and 0.95, from top to bottom. The overdensity oscillates between values close to 1 (represented as light tones (yellow in the color version)) at early times, where there are no lumps, to values close to 10 (dark tones (blue and purple in the color version)), where several concentrated lumps form at intermediate times. At later times lumps dissolve and the overdensity decreases back to values close to unity. (Right panel) Model M4, at scale factors $a = 0.35, 0.42, 0.53$, and 0.64, from top to bottom. The neutrino lumps start growing at early times and merge progressively into larger and more concentrated structures. At the end, almost all neutrinos are attracted to a single, very massive lump.

relativistic velocities. Subsequently, the lumps dissolve and form again periodically, as described in detail in Refs. [18,19]. We demonstrate this behavior in the left panel of Fig. 1. The repeated acceleration epochs heat the neutrino fluid to a huge effective temperature, such that neutrinos have again an almost relativistic equation of state during alternating periods of time.

By contrast, the behavior for large neutrino masses is qualitatively different. The concentration of the lumps continues to grow after their first formation. Lumps merge and typically do not dissolve. The neutrino number density contrast reaches high values at late times. This is demonstrated in the right panel in Fig. 1 for an average value of the neutrino mass $m_{\nu,\mathrm{av}} = 0.4$ eV in the range $0.4 < a < 0.6$. This behavior resembles the one found for a constant cosmon-neutrino coupling in [16–18].

Because of the increasing value of the concentration and the increasing cosmon-neutrino coupling, the characteristic time scale becomes very short and the gradients very large. This exceeds the present numerical capability of our simulations, typically at a value of the scale factor somewhat larger than $a = 0.6$. In Fig. 2 we show snapshots for two different values of neutrino masses shortly before the simulation breaks down.

The transition between the "heating regime" for small neutrino masses and the "concentration regime" for large neutrino masses occurs in the range $\langle m_\nu \rangle [0.4:0.6] \approx 0.07$–$0.14$ eV, where the time average is taken for $0.4 < a < 0.6$. The present value of the neutrino mass can be substantially larger due to oscillations and the continued increase of the mass and the temperature. For example, the phenomenologically viable model with $\langle m_\nu \rangle [0.4:0.6] = 0.07$ eV corresponds to a present neutrino mass of around 0.08 eV, but the time oscillations grow the neutrino mass to values of up to 0.5 eV for very short intervals in the scale factor a (compare to Fig. 5 below).

In Fig. 1 we show the distribution of the number (over) density contrast $\delta n_\nu(\vec{x}) \equiv n_\nu(\vec{x})/\bar{n}_\nu - 1$ at four different times and for two different models considered here, namely, M2 (left panels) and M5 (right panels). For M2 as well as for models with smaller masses (not shown here), the neutrino lumps form and dissolve very quickly. The lumps are never stable and neutrinos accelerate to relativistic velocities when they fall into the gravitational potentials. The small lumps are also distributed homogeneously across the simulation box (see the third panel from the top on the right of Fig. 1). The lumps reach maximal number density contrasts of about $\delta n_\nu \approx 10$. For M5 and for bigger masses, the neutrino lumps become stable, accreting more and more particles with the passing of time and increasing their concentrations. This leads to strong backreaction effects, changing the background cosmological evolution. After some time, all of the neutrinos are concentrated in very big lumps, reaching very high values of $\delta_\nu \approx 50$–100, where $\delta_\nu \equiv \rho_\nu(\vec{x})/\bar{\rho}_\nu - 1$; see Fig. 2. After this point, the numerical framework for the growing neutrino quintessence evolution breaks down and we can no longer reliably solve the coupled system of equations.

V. COSMOLOGICAL EVOLUTION IN THE LIGHT NEUTRINO REGIME

As we have seen in the previous section, there is a qualitative difference between the cosmological evolution

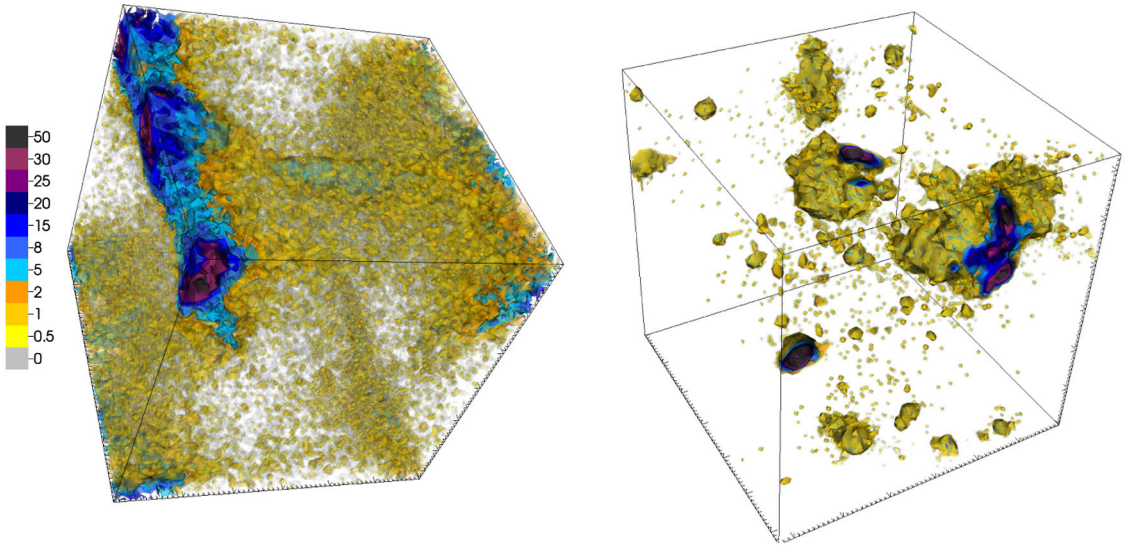

FIG. 2. Snapshots of the neutrino overdensity field $\delta_\nu(\vec{x})$ for models (top left) M4 and (bottom left) M6 at scale factors of $a = 0.64$, and 0.62, respectively. In these models, neutrino lumps cluster into large stable structures with a high concentration, starting from a bottom-up approach, as was shown for model M4 in Fig. 1. Neutrino structures occupy large parts of the simulation box, corresponding to scales of ~50 Mpc. At these scale factors, the forces introduced by the cosmon coupling are too strong to be resolved by our numerical approach, and our simulation breaks down.

of a model with a light or a heavy neutrino mass, the boundary being a present neutrino mass value of roughly ≈0.5 eV (calculated in linear theory). In this section we explore more in detail the evolution of background quantities in the light mass model M2, whose parameters are shown in detail in Table I for the linear calculation in nuCAMB (the top panel) and for the N-body computation (the bottom panel). We study in detail the differences appearing in the evolution of background quantities when nonlinear physics and backreaction are taken into account.

The standard definition for the homogeneous energy density fraction of the cosmon field ϕ is

$$\Omega_\phi = \frac{8\pi G}{3H^2}\bar{\rho}_\phi, \tag{27}$$

where $\bar{\rho}_\phi$ is the background energy density of a homogeneous scalar field $\bar{\rho}_\phi = K(\phi) + V(\phi)$ and $K(\phi)$ its kinetic energy. In linear theory, the homogeneous term would be the only term entering into Ω_ϕ; on the contrary, within the N-body simulation, the field is nonhomogeneous and the combined energy density of the coupled neutrino-cosmon fluid also receives a contribution from the perturbations $\delta\rho_\phi$ of the nonhomogeneous cosmon field, given by Eq. (18). The important quantity determining the evolution of a dynamical dark energy is not the energy density of the cosmon alone, but the energy density of the combined cosmon-neutrino fluid, given by

$$\Omega_{\phi+\nu} = \frac{8\pi G}{3H^2}(\bar{\rho}_\phi + \bar{\rho}_\nu). \tag{28}$$

The average energy density of the neutrinos is not individually conserved and its evolution is given by the continuity equation with a coupling term on the rhs [17,22],

$$\rho_\nu + 2\mathcal{H}\rho_\nu = -\beta(\phi)\phi'\rho_\nu, \tag{29}$$

where ϕ' is the time derivative of the field with respect to conformal time τ. The corresponding equation of state of the coupled fluid can then be defined as the sum of the pressure components divided by the sum of the density components:

$$w_{\nu+\phi} = \frac{\bar{p}_\phi + \bar{p}_\nu}{\bar{\rho}_\phi + \bar{\rho}_\nu}. \tag{30}$$

In the literature [4,26–28], there are several definitions of the effective equation of state or the observed equation of state in the case in which the scalar field is coupled to other particles. We argue that (30) is actually the equation of state one would observe from the evolution of the Hubble function (i.e., with supernovae and standard candle methods of redshift distance measurements). In Appendix B we comment further on this and show a comparison between the "observed" and theoretical equation of state of dark energy in Fig. 10.

In Fig. 3 we plot for model M2 the background evolution of the neutrino energy density Ω_ν (the orange lines) and the combined cosmon + neutrino fluid energy density $\Omega_{\nu+\phi}$ (the blue lines), as defined in Eq. (28). The dashed lines correspond to the linear computation in nuCAMB, while the solid lines correspond to the results of the N-body simulation. One can see that the effect of nonlinearities and backreaction is quite small and is mostly just visible as a phase shift in the oscillations of Ω_ν, which is due to the dynamics of the oscillating lumps, which alter the field-dependent mass of the neutrinos as a function of time and space. The same trend is observed in model M1 (not shown here). This behavior tells us that, for small neutrino masses, the effects of backreaction on the background evolution are practically negligible and a linear computation is enough to analyze those models further, with a considerable simplification with respect to the joint linear and nonlinear analysis done in [15].

We show in Fig. 4 the neutrino equation of state w_ν (the orange lines) as well as the combined cosmon-neutrino fluid equation of state $w_{\nu+\phi}$, as defined in Eq. (30) (the blue lines), for the case of both the linear computation with nuCAMB (the dashed lines) and the nonlinear computation (the solid lines). In the linear analysis, the neutrinos are treated initially as relativistic particles: as the mass increases, they become more and more nonrelativistic, reaching a w_ν of exactly zero at late times. On the contrary, the N-body simulation is able to follow the oscillations in the equation of state of the neutrinos, which are caused by the fact that neutrinos get accelerated to relativistic

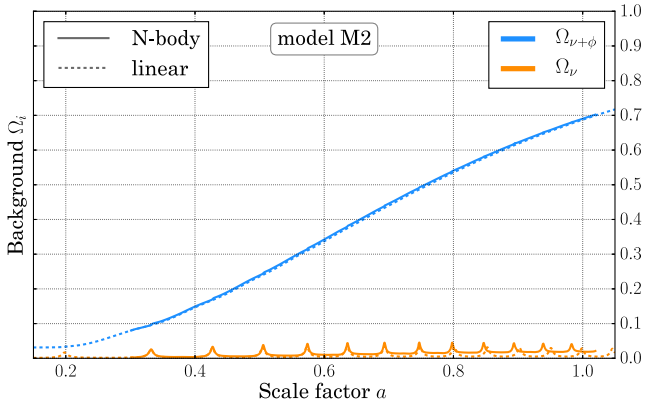

FIG. 3. Evolution of $\Omega_{\phi+\nu}$ (darker grey lines, blue in the color version) and Ω_ν (the lighter grey lines (orange in the color version)) for model M2, compared between the linear output from nuCAMB (the dashed lines) and the nonlinear calculation of the N-body simulation (the solid lines). The total cosmon-neutrino fluid has the same background evolution in the simulation as in the linear calculation. The neutrino energy density is somewhat larger in the simulation and shows a phase shift in its oscillations, as discussed in the text.

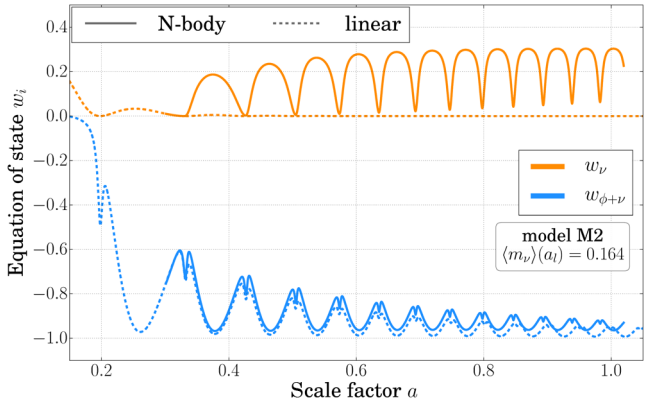

FIG. 4. Equation of state of the combined neutrino-cosmon fluid $w_{\phi+\nu}$ (darker lines (blue in the color version)) and equation of state of neutrinos w_ν (lighter grey lines (orange in the color version)). We compare the linear output (the dashed lines) to the nonlinear one obtained from the N-body simulation (the solid lines) for model M2. This model has a time averaged rms mass $\langle m_\nu\rangle(a_l) = 0.164$, where $a_l = 0.9$ in the label denotes the center of the time interval $a = [0.8\text{–}1.0]$ used to take the average. For w_ν, the linear output does not capture the oscillating equation of state of neutrinos due to the formation of structures, while, for $w_{\phi+\nu}$, both codes agree relatively well. At late times, the equation of state predicted by the simulation has a somewhat higher value and is phase shifted due to the heating of the neutrino fluid.

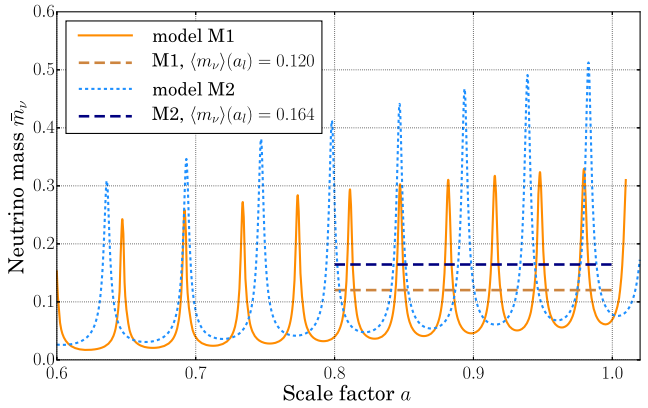

FIG. 5. Neutrino mass $\bar{m}_\nu$ (average over simulation volume) in model M2 (dotted line, blue in the color version) and model M1 (solid line, orange in the color version), as a function of the scale factor a, for the N-body simulation. The horizontal lines show the time averaged rms value at a late time $a_l = 0.9$, denoting the center of the time interval of $[0.8:1.0]$ considered for taking the average. For model M2, the time averaged neutrino mass is $\langle m_\nu\rangle(a_l) = 0.164$ (dark grey dashed line, dark blue in the color version), while for model M1 it is somewhat smaller $\langle m_\nu\rangle(a_l) = 0.120$ (light grey dashed line, dark orange in the color version). One can observe that the oscillation frequency is higher for the smaller $\langle m_\nu\rangle$ mass and the peaks are higher for the larger $\langle m_\nu\rangle$. The present neutrino masses of the two models calculated in linear theory differ by an order of magnitude; on the contrary, the time averaged masses are very close to each other.

velocities when they fall into deep gravitational and cosmon potentials. Once they are in these lumps and they have acquired high speeds, their pressure increases and they tend to escape again from these lumps, causing the oscillating neutrino structures. When they are far away from the cosmon potentials, their velocities decrease and they become nonrelativistic again. The fifth force acting among the neutrinos attracts them again to the cosmon potential wells, and the whole cycle repeats itself.

For the combined equation of state $w_{\nu+\phi}$, we find that the simulation predicts a slightly higher value than the linear one; this can be explained by studying how the neutrino fluid is heated due to the strong oscillations of the lumps. By falling repeatedly in the cosmon potential wells and increasing their kinetic energy, the neutrinos' temperature increases and, therefore, the neutrinos do not manage to become again completely nonrelativistic. This can be seen in the dashed orange lines of plot 4, where the curve of w_ν does not touch the zero axis after $a \approx 0.5$. We will see in Sec. VI that the neutrinos depart from their initial Fermi-Dirac distributions and reach temperatures which are high compared to the photon background.

In Fig. 5, we show the evolution of the spatial average of the neutrino mass in the N-body simulation as a function of the scale factor a. One can see that the value of $\bar{m}_\nu$ varies along an order of magnitude, from approximately 10^{-2} to 10^{-1}, throughout a cosmological time interval. Because of a phase shift in the oscillation pattern, which sets in at around $a \approx 0.8$, the present day value of the average neutrino mass can be quite different from the one estimated with the linear analysis (and this change depends on the precise parameters of the model), so that the best estimate for the average cosmological neutrino mass today is a time average of $\bar{m}_\nu(\phi)$ at late times where $a = 0.8\text{–}1.0$. We can see that the big discrepancies between the masses of models M1 and M2 calculated in linear theory (e.g., Table I) are washed away when nonlinearities and backreaction effects are taken into account, i.e., for small neutrino masses. Even if the present neutrino masses for models M1 and M2 differ by an order of magnitude in linear theory, we find a very similar time averaged value between the two models in the N-body simulation: $\langle m_\nu\rangle[0.8:1.0] = 0.120$ and $\langle m_\nu\rangle[0.8:1.0] = 0.164$, respectively. The oscillation pattern of the neutrino mass for the more massive model (M2) contains higher peaks and has a smaller frequency than the oscillations in the less massive model (M1). For other models, this comparison can be seen in Table I.

VI. HEATING OF THE NEUTRINO FLUID

The repeated acceleration of neutrinos to relativistic velocities during the periods of lump formation and dissolution lead to an effective heating of the neutrino fluid. While we do not expect a thermal equilibrium distribution of neutrino momenta and energies, it is interesting to investigate how close the distribution is to the Fermi-Dirac distribution of a free gas of massive

neutrinos. This distribution depends on only two parameters, the neutrino mass and the temperature. At a given time, we associate the neutrino mass to the space averaged neutrino mass. The temperature can be associated to the mean value of the momentum.

The energy of a relativistic particle is given by

$$E(p,m) = \sqrt{p^2 + m^2}, \tag{31}$$

while its kinetic energy $E_k = E(p,m) - m$. Equivalently, the kinetic energy is defined as

$$E_k = \int \vec{v} \cdot \mathrm{d}\vec{p}, \tag{32}$$

which yields $E_k = m(\gamma - 1)$ and reduces in the limit of very small velocities ($v \lll c$) to the usual $E_k = mv^2/2$. From there, the Fermi-Dirac distribution as a function of momentum $p = |\vec{p}|$ can be obtained in the standard way. It depends on m and T. For $m \ll T$, it can be approximated by the relativistic distribution, while for $m \gg T$ we recover the Maxwell-Boltzmann distribution. The distribution of particle momenta is then given by

$$\mathcal{P}(p)\mathrm{d}p = \frac{4\pi p^2}{(1 + e^{(E(p,m)-\mu)/T})}\mathrm{d}p, \tag{33}$$

where the factor 4π comes form the angular integration of the three-dimensional momentum. In the ultrarelativistic limit, we can analytically integrate the momentum p over its distribution equation (33) and invert $\bar{p}(\bar{T})$ to yield the mean temperature as a function of the mean momentum:

$$\bar{T} = \frac{180\zeta(3)}{7\pi^4}\bar{p}. \tag{34}$$

We neglect the chemical potential in (33) because the exponential term in the denominator is 2 or 3 orders of magnitude larger than unity. Since, in our case, the average momentum and mass of the neutrinos are of the same order, we cannot use either a nonrelativistic or an ultrarelativistic limit. We need to consider both the mass and the momentum in the relativistic energy equation (31). Therefore, for each model and each time, we numerically find $\bar{T}$ as a function of the mean momentum $\bar{p}$.

We extract for $a = 1$ the temperatures

$$\begin{aligned} \bar{T} &= 0.077 \text{ eV} \quad (\mathrm{M1}, \bar{m}_\nu = 0.2404), \\ \bar{T} &= 0.065 \text{ eV} \quad (\mathrm{M2}, \bar{m}_\nu = 0.2327). \end{aligned} \tag{35}$$

They are higher by a factor 327 (M1) or 276 (M2) as compared to the cosmic microwave background (CMB) photon temperature 2.35×10^{-4} eV. This demonstrates the unconventional heating of the neutrino fluid due to the formation and dissolution of lumps. The high temperatures are connected with the almost relativistic equation of state of the neutrinos seen in Fig. 4. Overall, the observed momentum distributions come rather close to the thermal equilibrium distribution. This also holds for the distribution of kinetic energies. With the bulk quantities as momenta and kinetic energies roughly distributed thermally, this is an example of prethermalization [29].

In Fig. 6, we fit the distribution of momenta of the neutrino particles on the grid (shown with a histogram) with a Fermi-Dirac distribution. The actual distribution of momenta fits the thermal equilibrium distribution very well. At later times (the orange shade), the fit is slightly less good: neutrinos might be accelerating towards or away from lumps, giving them an extra kick that shifts the peak of the distribution of momenta.

When comparing the equation of state of the neutrinos obtained from the N-body simulation to a neutrino equation of state $w_\nu = p_\nu/\rho_\nu$, using our Fermi-Dirac fit to the particle distribution and Eqs. (15) and (14), we get very

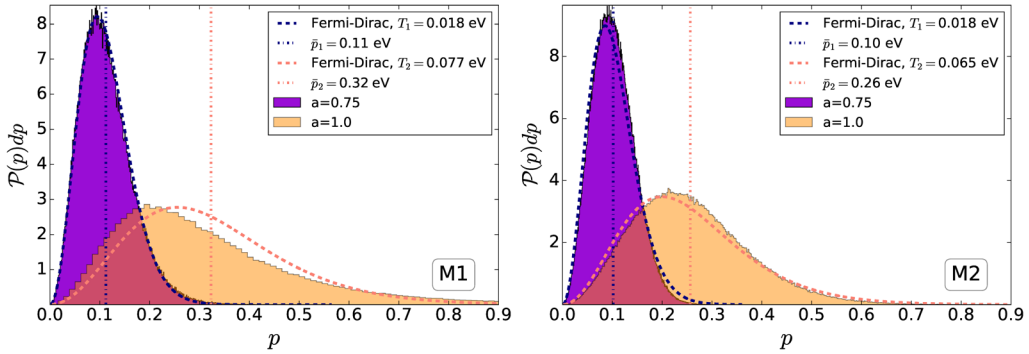

FIG. 6. Distribution of the momenta of the neutrino particles in the simulation for two different times, $a = 0.75$ (the dark shade (purple in the color version)) and $a = 1.0$ (the lighter shade (orange in the color version)), compared to a Fermi-Dirac distribution with a temperature given by the mean of the distribution (the dashed lines). (Left panel) For model M1, the Fermi-Dirac fits very well for temperatures of $\bar{T} = 0.018$ eV and $\bar{T} = 0.077$ eV, respectively, for each scale factor. (Right panel) For model M2, the fit is also good, with the corresponding temperatures being $\bar{T} = 0.018$ eV and $\bar{T} = 0.065$ eV. The CMB photon temperature is 2.35×10^{-4} eV, this means that the nonlinear cosmon-neutrino interactions heat the neutrino background by more than a factor of 100.

good agreement, taking into account that, for the Fermi-Dirac fit, we are neglecting the spatial variation of the neutrino mass $m_\nu(\phi)$. For model M2 at the scale factor $a = 0.75$, we obtain from the N-body simulation a neutrino equation of state of $w_\nu = 0.081$, while, using the Fermi-Dirac fit to the distribution of particles with a mean temperature of $\bar{T} = 0.018$ eV and an average neutrino mass $\bar{m}_\nu = 0.1835$, the proper calculation yields $w_\nu = 0.086$. For a later time, at $a = 1.0$ the N-body simulation gives us a value of $w_\nu = 0.207$, while the Fermi-Dirac fit with a mean temperature of $\bar{T} = 0.065$ eV and an average neutrino mass $\bar{m}_\nu = 0.2327$ amounts to a neutrino equation of state of $w_\nu = 0.182$.

To visualize the evolution of w_ν, we can observe from Fig. 4 that neutrinos in the N-body simulation start as nonrelativistic particles and oscillate between being almost relativistic and completely nonrelativistic in the interval $a = [0.3, 0.6]$. However, at later times where $a \gtrsim 0.7$, the neutrino equation of state still oscillates but never reaches a value of zero again. This is in agreement with our description of the heating of the neutrino fluid. Since the mean temperature of the neutrino fluid is increasing with time—and therefore its mean kinetic energy and pressure—the minimum of the oscillations of the neutrino equation of state increases also in time and departs from zero, once neutrinos are heated to very high temperatures due to the collapsing and dissolving of the neutrino-cosmon lumps.

VII. GRAVITATIONAL POTENTIALS OF NEUTRINO LUMPS

The gravitational potential Φ is a good measure of the physics going on in structure formation. We know, from observational constraints, that Φ is of the order of 10^{-5} on cosmological scales [14,15]. In ΛCDM, the gravitational potential is sourced mainly by dark matter perturbations. In Figs. 7 and 8, we show that, for models with small neutrino masses, the neutrino contribution to Φ remains several orders of magnitude smaller than the CDM contribution, at all scales and at all times. Moreover, one can observe an oscillation in time of the neutrino gravitational potential. For models with large neutrino masses, the neutrino contribution grows monotonically with time. At large scales $k \lesssim 0.3$ h/Mpc and at late times, the neutrino lump induced potential dominates over the cold dark matter gravitational potential. This renders the total potential $\Phi_{\rm tot}$ too big to be compatible with present cosmological constraints.

We show the scale dependence of the total gravitational potential and the neutrino-induced gravitational potential Φ_ν at two different cosmic time scales, $a = 0.4$ and $a = 0.65$, in Fig. 7. For $a = 0.4$ (the solid lines), the neutrino contribution is still subdominant for both model M2 and model M5; this changes at $a = 0.65$ for model M5 (the bottom panel). For model M2, the total gravitational potential decreases in time, as is expected due to the effect

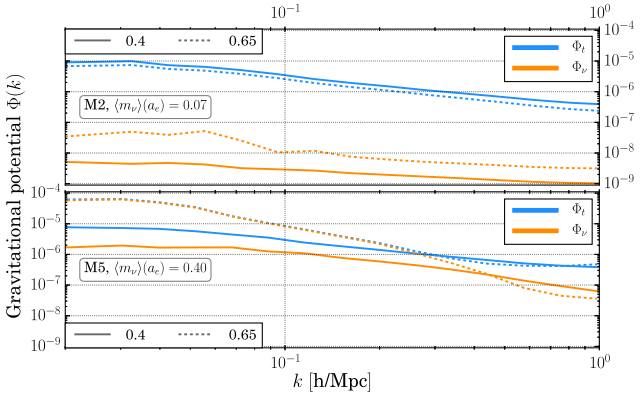

FIG. 7. Power spectra of the total gravitational potential Φ_t (the darker grey lines (blue in the color version)) and of the neutrino contribution Φ_ν (the lighter grey lines (orange in the color version)) for models M2 and M5 at the scale factors $a = 0.40$ (the solid lines) and $a = 0.65$ (the dashed lines), as a function of scale. Model M2 has a rms time averaged neutrino mass $\langle m_\nu\rangle(a_e) = 0.07$, where $a_e = 0.5$ stands for the central time in the interval $a = [0.4\text{–}0.6]$ used to take the average. Model M5 has in the same interval a higher rms mass of $\langle m_\nu\rangle(a_e) = 0.40$. In the first model, Φ_t at large scales is of the order of 10^{-5}, while Φ_ν is 3 to 4 orders of magnitude smaller at both cosmological times. For model M5, in which neutrino lumps are stable and growing, one sees that, at large scales, the total Φ_t starts with a value of 10^{-5} at $a = 0.4$, but it reaches 10^{-4} at later times. At $a = 0.65$, the neutrino contribution is dominant and neutrino structures have migrated from small scales to large scales, as can be seen from the dip in Φ_ν at modes where $k = 0.2 - 1.0$ h/Mpc.

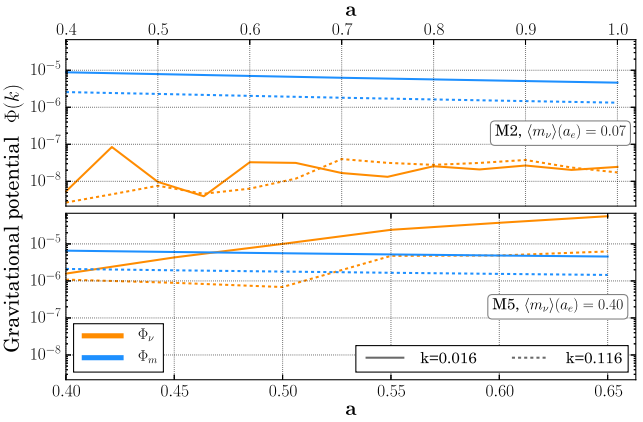

FIG. 8. Power spectra of the matter gravitational potential Φ_m (the darker grey lines (blue in the color version)) and of the neutrino contribution Φ_ν (the lighter grey lines (orange in the color version)) at two different scales, $k = 0.016$ (the solid lines) and $k = 0.116$ (the dashed lines) as a function of scale factor a with different scales on the top and bottom axis. For model M2, the matter gravitational potential Φ_m is, at most, 10^{-5} at all times, while the neutrino contribution is 2 to 3 orders of magnitude smaller and displays time oscillations. In clear contrast, the neutrino contribution from model M5 for very large scales, reaches and dominates over the matter contribution for $a \gtrsim 0.5$ and pushes the total Φ to high values that would be ruled out by observations; see also Fig. 7. The rms neutrino mass has been taken in the same interval range as for Fig. 7, where $a_e = 0.5$.

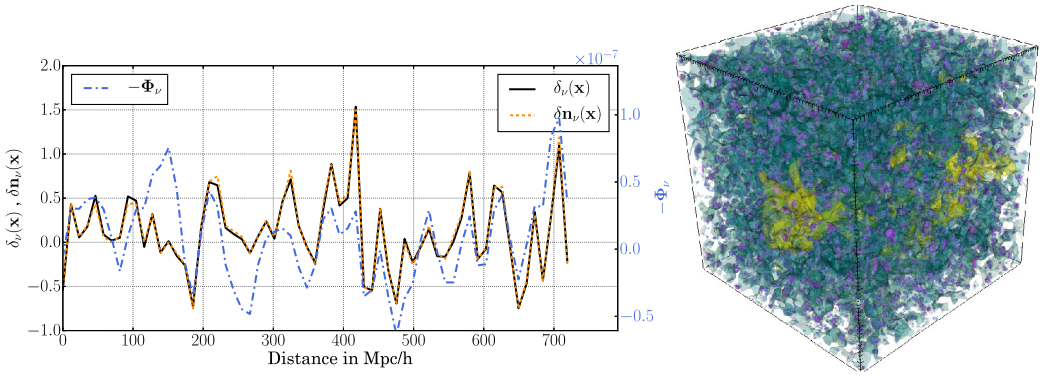

FIG. 9. (Left panel) Line plot through the main diagonal of the simulation box for model M2 at $a = 0.75$. The negative of the neutrino contribution to the gravitational potential Φ_ν (the dot-dashed lighter lines (blue in the color version)) oscillates in the range $\pm 1.0 \times 10^{-7}$. This is correlated to the neutrino density contrast (the black solid lines) and the number density contrast $\delta n_\nu = n_\nu(\vec{x})/\bar{n}_\nu - 1$ (the darker dashed lines (orange in the color version)), reaching values of up to 1.5. (Right panel) Snapshot of the same simulation, showing a equipotential contour of the gravitational potential, for $\Phi_\nu = +1.0 \times 10^{-7}$ in lighter areas (yellow in the color version), and the small but dense neutrino lumps in darker areas (blue, purple and red in the color version), corresponding to density contrasts δn_ν of 1.5, 2.0, and 4.0, respectively.

of dark energy, while Φ_ν increases especially at large scales. For model M5, since the neutrino contribution dominates at $a = 0.65$, the total gravitational potential is raised to values of 10^{-4} at large scales, while, at small scales ($k \gtrsim 0.4$), the neutrino contribution is still subdominant.

In Fig. 8, we show the power spectra of the total gravitational potential Φ (the blue lines) and of the neutrino contribution to it (the orange lines) at two different scales, $k = 0.016$ (the solid lines) and $k = 0.116$ (the dashed lines), as a function of the scale factor a. For model M2, corresponding to an average early time neutrino mass of 0.07 eV, the total gravitational potential $\Phi(k)$ is 10^{-5} at all times, while the neutrino contribution is 2 to 3 orders of magnitude smaller and shows time oscillations. In clear contrast, the neutrino contribution from model M5 (corresponding to an average early time neutrino mass of 0.40 eV) for very large scales reaches and dominates over the matter contribution (at $a \gtrsim 0.5$) and pushes the total Φ to high values that would be ruled out by observations. This is due to the fact that neutrino lumps do not dissolve but rather grow with continuously growing concentration and higher gravitational potential.

There is also anticorrelation between the neutrino structures and the neutrino-induced gravitational potential, as expected from the fact that neutrinos will tend to fall into gravitational potential wells. In the left panel of Fig. 9, we plot the values of the neutrino number density contrast $\delta n_\nu = n_\nu(\vec{x})/\bar{n}_\nu - 1$ and the negative neutrino-induced gravitational potential Φ_ν, along a diagonal line through the simulation box. The correlation of peaks and troughs (corresponding to an anticorrelation of δn_ν and Φ_ν) is very clear, and it is valid even for small substructures of the order of a few megaparsecs. By plotting the neutrino density contrast δ_ν, we also show that, at the time $a = 0.75$, the neutrino number density and the energy density are proportional, meaning that neither local mass variations or relativistic speeds are having any effect in the neutrino total energy. In the right panel of Fig. 9, we visualize the neutrino-induced gravitational potential as a yellow region marking the equipotential surface $\Phi_\nu = +1.0 \times 10^{-7}$ and the neutrino number overdensity structures colored blue, purple, and red, corresponding to density contrasts δn_ν of 1.5, 2.0, and 4.0, respectively. For this model (M2) and at this specific time, the neutrino structures are spread almost homogeneously throughout the simulated volume.

VIII. CONCLUSIONS

We have investigated the dynamics of neutrino lumps in growing neutrino quintessence and how it depends on the mass of neutrinos. As a main result of this paper, we have found a characteristic divide in the qualitative behavior between small and large neutrino mass.

For light neutrino masses, the combined effects of oscillations in the neutrino masses and the cosmon-neutrino coupling lead to rapid formation and dissociation of the neutrino lumps. The concentration in the neutrino structures never grows to very large overdensities. As a consequence, backreaction effects remain small. The effects of lump formation and dissociation lead to an effective heating of the neutrino fluid to temperatures much higher than the photon temperature. Because of this heating, the neutrino equation of state again becomes close to the one for relativistic particles. For a small present average neutrino mass $m_\nu = 0.06$ eV, it was found previously [15] that the cosmology of growing neutrino quintessence resembles very closely a cosmological constant, making differences to the ΛCDM model difficult to detect. We extend this qualitative feature to a whole range of light neutrino masses.

For large neutrino masses, one finds a qualitatively different behavior. Big neutrino lumps form due to the strong cosmon-mediated fifth force between neutrinos. These lumps are stable and keep growing in concentration and density. The strong clumping of the cosmic neutrino background induces large backreaction effects on the overall cosmic evolution. As a result, the combined cosmon-neutrino fluid does not act effectively as a cosmological constant anymore, and compatibility with observations is difficult to achieve. This situation is similar to the case of a constant cosmon-neutrino coupling [20].

The divide in the characteristic behavior reflects the competition between heating of the neutrino fluid and lump concentration. We have not yet established a quantitatively accurate value of the parameter $\hat{m}_\nu$, where the divide is located, since the numerics are rather time consuming. In principle, this divide will lead to an upper bound on the present neutrino mass, as seen in terrestrial experiments. For models in the vicinity of model M2, which seem compatible with observations thus far, spatial average neutrino masses as large as 0.5 eV can occur at the peak of oscillations; cf. Fig. 5. We note that, if we live inside a neutrino lump, the neutrino mass will be reduced in comparison to the cosmological value.

We have further computed the strength of the neutrino-induced gravitational potential. For light masses, this potential is found to be rather small, rendering a detection of the neutrino lumps difficult. As neutrino masses increase towards an intermediate mass region, before reaching the heavy mass range incompatible with observation, the neutrino-induced gravitational potentials will get stronger. By continuity, we expect that, in the intermediate mass region, the clumped neutrino background becomes observable.

ACKNOWLEDGMENTS

We would like to thank Florian Führer for the insightful help and the discussions about the model and its simulation. V. P. and S. C. acknowledge support from the Heidelberg Graduate School for Fundamental Physics. The authors acknowledge support by the state of Baden-Württemberg for the computational capabilities offered through the bwHPC. This research has been supported by ERC-AdG-290623DFG and through the Grant No. TRR33, "The Dark Universe."

APPENDIX A: INITIAL PARAMETERS FOR GENERATING THE MODELS IN nuCAMB AND IN THE N-BODY SIMULATION

TABLE II. Table of initial parameters for each model, computed with nuCAMB. $\tilde{m}_\nu$ is the neutrino mass amplitude used in the simulations, $\hat{r}_{\nu\mathrm{eV}}$ is the neutrino mass unit conversion factor between the simulations and nuCAMB. V_i is the initial value of the cosmon potential.

CAMB values	M1	M2	M3	M4	M5	M6
Input $(\Omega_\nu h^2)$	0.048	0.048	0.075	0.018	0.038	0.098
$\tilde{m}_\nu$ amplitude factor	8.35×10^{-5}	2.0×10^{-4}	6.0×10^{-4}	9.9×10^{-3}	8.8×10^{-3}	8.8×10^{-3}
Input $\hat{r}_{\nu\mathrm{eV}}$ factor	1.5045	1.5045	2.3508	0.5642	1.1911	3.0718
V_i	0.99×10^{-7}	0.99×10^{-7}	0.99×10^{-7}	0.99×10^{-7}	0.99×10^{-7}	0.99×10^{-7}

TABLE III. Table of numerical parameters for each N-body simulation run. Several tests were performed varying these parameters, but the overall behavior for the purposes of this paper was the same. We also tested model M2 with grid sizes of 128 and 8 times the number of particles, not noticing any qualitative difference in the dynamics. Only deviations of the order of 10% in perturbation quantities were observed when varying the grid size or the number of particles.

N-body parameters	Values	Meaning
L	428	Box side length in Mpc/h
N_g	64	Grid size per dimension
N_{pdm}	262 144	Number of dark matter particles in the simulation
$N_{p\nu}$	524 288	Number of neutrino particles in the simulation
$\mathrm{ngs}_{\mathrm{acc}}$	1.0×10^{-5}	Numerical accuracy for the Newton-Gauß-Seidel (NGS) solver

APPENDIX B: THE EFFECTIVE AND OBSERVED EQUATION OF STATE OF DARK ENERGY

The equation of state w of a species is defined in terms of its pressure and density as

$$w = \frac{p}{\rho}. \tag{B1}$$

For the case of coupled species, there have been several definitions in the literature (cf. [4,26–28]). This is due to the fact that when there is an exchange of energy and momentum between a particle and a scalar field, the time evolution of matter does not correspond anymore to the volume dilution rule $\rho(a) = \rho_0 a^{-3}$. Therefore, the equation of state of the dark energy field will not be as simple as the equation of state of a homogeneous scalar field, namely,

$$w_\phi = \frac{p_\phi}{\rho_\phi} = \frac{(1/2a^2)\dot{\phi}^2 + V(\phi)}{(1/2a^2)\dot{\phi}^2 - V(\phi)}. \tag{B2}$$

In [4,26], two definitions of the equation of state (EOS) of dark energy were investigated. The first one, called the effective EOS $w_{\rm eff}$, is given by

$$w_{\rm eff} \equiv w_\phi + \frac{\beta\dot{\phi}}{3H}\frac{\rho_\nu}{\rho_\phi}, \tag{B3}$$

and the second one, named the "apparent" EOS $w_{\rm ap}$, is defined by

$$w_{\rm ap} \equiv \frac{w_\phi}{1+x}, \tag{B4}$$

with

$$x = -\frac{\rho_{\nu,0}}{a^3\rho_\phi}\left[\frac{m_\nu(\phi)}{m_\nu(\phi_0)} - 1\right], \tag{B5}$$

where a 0 subscript denotes quantities at $z = 0$. Notice that, by construction, $w_{\rm ap}$ at the present epoch is identical to w_ϕ, and also that $w_{\rm ap}$ can be smaller than -1. We find that neither of these two definitions of EOSs describes the dynamical dark energy field present in our model.

Since, in our model, the neutrino and cosmon field behave together as a tightly coupled fluid, we are interested in the conserved equation of state for the combined fluid. This is given by the sum of both contributions from the pressure divided by the sum of both densities. Therefore, we define $w_{\nu+\phi}$ as

$$w_{\nu+\phi} \equiv \frac{\bar{p}_\phi + \bar{p}_\nu}{\bar{\rho}_\phi + \bar{\rho}_\nu}. \tag{B6}$$

This definition should agree with what we can extract directly from observations of the Friedmann equation. The equation of state $w_{\rm DE}(z)$ of a general dark energy component that fulfills the continuity equation (if it is composed by two coupled fluids, the continuity equation is fulfilled for the sum of densities and pressures) appears in the Friedmann equation as

$$E^2(z) \equiv \frac{H^2(z)}{H_0^2} = \Big[\Omega_{r,0}(1+z)^4 + \Omega_{m,0}(1+z)^3 + \Omega_{\rm DE,0}\exp\left\{\int_0^z \frac{3(1+w_{\rm DE}(\tilde{z}))}{1+\tilde{z}}\,{\rm d}\tilde{z}\right\} + \Omega_{k,0}(1+z)^2\Big]. \tag{B7}$$

Moreover, in a flat Universe and with a negligible contribution from radiation, we can solve for $w_{\rm DE}(z)$ and obtain [30]

$$w_{\rm DE}(z) = \frac{(1+z)(E^2(z))' - 3E^2(z)}{3[E^2(z) - \Omega_{m,0}(1+z)^3]}. \tag{B8}$$

Thus, from background expansion observations, we can obtain a constraint on $w_{\rm DE}(z)$, provided we know from large-scale structure or CMB observations the present value of Ω_m. In Fig. 10, we compare the $w_{\rm DE}(z)$ obtained from Eq. (B8) and $w_{\nu\phi}(z)$, with both computed consistently within the N-body simulation. In the former case, numerical noise in the derivatives of $E(z)$ create certain scatter in $w_{\rm DE}(z)$ at late times.

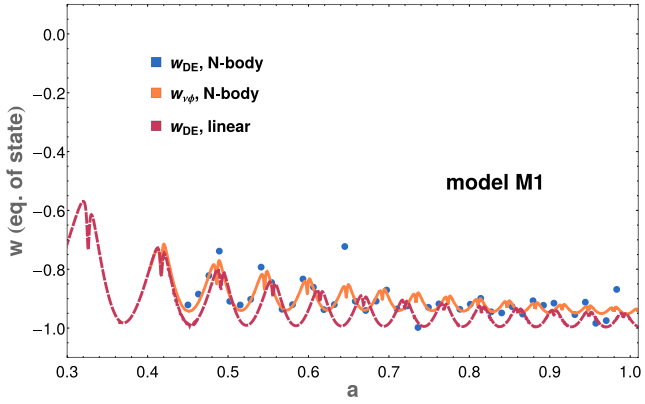

FIG. 10. Different $w(z)$ curves in the case of model M1 computed with the N-body simulation and compared to linear theory. The dark grey dashed lines (red in the color version) represent $w_{\rm DE}$ computed from the Hubble function which is an output of the linear code nuCAMB. The lighter solid line (orange in the color version), representing $w_{\nu+\phi}$ is computed using the standard pressure and density outputs from the simulation. The dark dots (blue in the color version) stand for some set of computed values of $w_{\rm DE}(z)$ obtained from the Hubble function that is calculated entirely within the N-body simulation. Because of numerical noise in the oscillating derivatives of $E(z)$, there is some scatter in the EOS obtained in this case.

[1] L. Amendola, M. Baldi, and C. Wetterich, Growing matter, Phys. Rev. D **78**, 023015 (2008).
[2] C. Wetterich, Growing neutrinos and cosmological selection, Phys. Lett. B **655**, 201 (2007).
[3] D. F. Mota, V. Pettorino, G. Robbers, and C. Wetterich, Neutrino clustering in growing neutrino quintessence, Phys. Lett. B **663**, 160 (2008).
[4] A. W. Brookfield, C. van de Bruck, D. F. Mota, and D. Tocchini-Valentini, Cosmology of mass-varying neutrinos driven by quintessence: Theory and observations, Phys. Rev. D **73**, 083515 (2006); **76**, 049901(E) (2007).
[5] G. La Vacca and D. F. Mota, Mass-varying neutrino in light of cosmic microwave background and weak lensing, Astron. Astrophys. **560**, A53 (2013).
[6] X.-J. Bi, B. Feng, H. Li, and X. Zhang, Cosmological evolution of interacting dark energy models with mass varying neutrinos, Phys. Rev. D **72**, 123523 (2005).
[7] R. Fardon, A. E. Nelson, and N. Weiner, Dark energy from mass varying neutrinos, J. Cosmol. Astropart. Phys. 10 (2004) 005.
[8] D. B. Kaplan, A. E. Nelson, and N. Weiner, Neutrino Oscillations as a Probe of Dark Energy, Phys. Rev. Lett. **93**, 091801 (2004).
[9] C. Spitzer, Stability in MaVaN models, arXiv:astro-ph/0606034.
[10] R. Takahashi and M. Tanimoto, Speed of sound in the mass varying neutrinos scenario, J. High Energy Phys. 05 (2006) 021.
[11] F. Simpson, R. Jimenez, C. Pena-Garay, and L. Verde, Dark energy from the motions of neutrinos, arXiv:1607.02515.
[12] N. Wintergerst and V. Pettorino, Clarifying spherical collapse in coupled dark energy cosmologies, Phys. Rev. D **82**, 103516 (2010).
[13] N. Wintergerst, V. Pettorino, D. F. Mota, and C. Wetterich, Very large scale structures in growing neutrino quintessence, Phys. Rev. D **81**, 063525 (2010).
[14] N. Brouzakis, V. Pettorino, N. Tetradis, and C. Wetterich, Nonlinear matter spectra in growing neutrino quintessence, J. Cosmol. Astropart. Phys. 03 (2011) 049.
[15] V. Pettorino, N. Wintergerst, L. Amendola, and C. Wetterich, Neutrino lumps and the cosmic microwave background, Phys. Rev. D **82**, 123001 (2010).
[16] Y. Ayaita, M. Weber, and C. Wetterich, Neutrino lump fluid in growing neutrino quintessence, Phys. Rev. D **87**, 043519 (2013).
[17] Y. Ayaita, M. Weber, and C. Wetterich, Structure formation and backreaction in growing neutrino quintessence, Phys. Rev. D **85**, 123010 (2012).
[18] M. Baldi, V. Pettorino, L. Amendola, and C. Wetterich, Oscillating non-linear large-scale structures in growing neutrino quintessence, Mon. Not. R. Astron. Soc. **418**, 214 (2011).
[19] Y. Ayaita, M. Baldi, F. Führer, E. Puchwein, and C. Wetterich, Nonlinear growing neutrino cosmology, Phys. Rev. D **93**, 063511 (2016).
[20] F. Führer and C. Wetterich, Backreaction in growing neutrino quintessence, Phys. Rev. D **91**, 123542 (2015).
[21] C.-P. Ma and E. Bertschinger, Cosmological perturbation theory in the synchronous vs. conformal Newtonian gauge, Astrophys. J. **455**, 7 (1995).
[22] M. Baldi, V. Pettorino, G. Robbers, and V. Springel, Hydrodynamical *N*-body simulations of coupled dark energy cosmologies, Mon. Not. R. Astron. Soc. **403**, 1684 (2010).
[23] A. Lewis, A. Challinor, and A. Lasenby, Efficient computation of CMB anisotropies in closed FRW models, Astrophys. J. **538**, 473 (2000).
[24] E. Puchwein, M. Baldi, and V. Springel, Modified-gravity-gadget: A new code for cosmological hydrodynamical simulations of modified gravity models, Mon. Not. R. Astron. Soc. **436**, 348 (2013).
[25] A. Schneider, R. Teyssier, D. Potter, J. Stadel, J. Onions, D. S. Reed, R. E. Smith, V. Springel, F. R. Pearce, and R. Scoccimarro, Matter power spectrum and the challenge of percent accuracy, J. Cosmol. Astropart. Phys. 04 (2016) 047.
[26] S. Das, P. S. Corasaniti, and J. Khoury, Superacceleration as signature of dark sector interaction, Phys. Rev. D **73**, 083509 (2006).
[27] F. Perrotta, C. Baccigalupi, and S. Matarrese, Extended quintessence, Phys. Rev. D **61**, 023507 (1999).
[28] F. Perrotta and C. Baccigalupi, On the dark energy clustering properties, Phys. Rev. D **65**, 123505 (2002).
[29] J. Berges, S. Borsanyi, and C. Wetterich, Prethermalization, Phys. Rev. Lett. **93**, 142002 (2004).
[30] L. Amendola and S. Tsujikawa, *Dark Energy: Theory and Observations* (Cambridge University Press, Cambridge, England, 2010).